Available online at www.sciencedirect.com
ScienceDirect
Trans. Nonferrous Met. Soc. China 27(2017) 2423−2433
Transactions of Nonferrous Metals Society of China
www.tnmsc.cn

Prediction of tri-modal microstructure under complex thermomechanical processing history in isothermal local loading forming of titanium alloy

Peng-fei GAO, He YANG, Xiao-guang FAN, Zhen-ni LEI, Yang CAI

State Key Laboratory of Solidification Processing, School of Materials Science and Engineering, Northwestern Polytechnical University, Xi'an 710072, China

Received 23 June 2016; accepted 18 September 2016

Abstract: To control the tri-modal microstructure and performance, a prediction model of tri-modal microstructure in the isothermal local loading forming of titanium alloy was developed. The staged isothermal local loading experiment on TA15 alloy indicates that there exist four important microstructure evolution phenomena in the development of tri-modal microstructure, i.e., the generation of lamellar α, content variation of equiaxed α, spatial orientation change of lamellar α and globularization of lamellar α. Considering the laws of these microstructure phenomena, the microstructure model was established to correlate the parameters of tri-modal microstructure and processing conditions. Then, the developed microstructure model was integrated with finite element (FE) model to predict the tri-modal microstructure in the isothermal local loading forming. Its reliability and accuracy were verified by the microstructure observation at different locations of sample. Good agreements between the predicted and experimental results suggest that the developed microstructure model and its combination with FE model are effective in the prediction of tri-modal microstructure in the isothermal local loading forming of TA15 alloy.

Key words: titanium alloy; isothermal local loading forming; complex thermomechanical processing history; tri-modal microstructure modelling

1 Introduction

The large-scale complex components of titanium alloy have gained increasing applications in aviation and aerospace fields due to their features of high performance, light mass and high reliability [1]. However, it is difficult to form these components due to the hard-to-deform properties of titanium alloy and the complex shape of component. The isothermal local loading forming technology proposed by YANG et al [2] integrates the advantages of local loading forming and isothermal forming, providing a highly attractive way to form these components. For the forming of these components, the shape and the microstructure are highly required to assure the service performance. GAO et al [3] found that the tri-modal microstructure, consisting of equiaxed α (α_p), lamellar α (α_l) and β transformed matrix (β_t), can be obtained through near-β forging combined with conventional forging in the isothermal local loading forming of titanium alloy. The tri-modal microstructure is a preferable microstructure morphology due to its good combination of strength, ductility and fracture toughness [4]. However, the parameters of tri-modal microstructure, such as the content, scale and distribution of each constituent phase, still play a critical role in the final performance. Therefore, it is essential to study the prediction of tri-modal microstructure in the isothermal local loading forming of titanium alloy, so as to quantitatively control the microstructure parameters and mechanical properties.

During the local loading forming, only partial workpiece is loaded and the component is formed by accumulating local deformation, as illustrated in Fig. 1 [3,5]. The workpiece undergoes multi-fire forging with complex temperature routes and severe unequal deformation, which makes the development of tri-modal microstructure undergo complicated microstructure

Foundation item: Projects (51605388, 51575449) supported by the National Natural Science Foundation of China; Project (B08040) supported by the "111" Project, China; Project (131-QP-2015) supported by the Research Fund of the State Key Laboratory of Solidification Processing (NWPU), China; Project supported by the Open Research Fund of State Key Laboratory of Materials Processing and Die & Mould Technology, Huazhong University of Science and Technology, China

Corresponding author: Peng-fei GAO; Tel/Fax: +86-29-88495632; E-mail: gaopengfei@nwpu.edu.cn

DOI: 10.1016/S1003-6326(17)60269-3

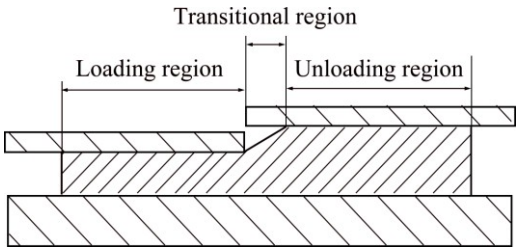

Fig. 1 Schematic diagram of local loading forming [3,5]

evolution phenomena. It involves the content variation of α_p, generation of α_l, spatial orientation change of α_l and globularization of α_l, and so on. Due to the complex microstructure evolution and coupling effects of multi-factors, it is difficult to predict the tri-modal microstructure in the isothermal local loading forming of titanium alloy.

By now, the existing microstructure prediction models for the isothermal local loading forming of titanium alloy are all aimed at the bi-modal microstructure which is produced at a simpler temperature route. LI et al [6] predicted the α_p grain size of bi-modal microstructure during the isothermal local loading forming of TA15 alloy by coupling an artificial neural networks (ANN) based microstructure model into the finite element (FE) model. FAN et al [7] established the through-process microstructure evolution model of bi-modal microstructure for the local loading forming of titanium alloy using internal state variable (ISV) method. It can predict the volume fraction and grain size of α_p. However, the production and evolution of α_l, an important constituent phase of the tri-modal microstructure, are not considered in the above models. GAO et al [8] and SUN et al [9] developed an ANN model to predict the content and grain size of α_p, and the content and thickness of α_l in the double heat treatments of TA15 alloy. However, they don't consider the spatial orientation change of α_l and globularization of α_l, which are important microstructure evolution phenomena for the development of tri-modal microstructure in isothermal local loading forming. Therefore, it is still needed to develop the prediction model of tri-modal microstructure under complex thermomechanical processing history in the isothermal local loading forming of titanium alloy.

In this work, the development mechanisms and rules of tri-modal microstructure in the isothermal local loading were revealed based on the staged experiments. A microstructure model was developed to correlate the parameters of tri-modal microstructure and deformation conditions. Then, the microstructure model was successfully implemented into FE model to achieve the prediction of tri-modal microstructure during isothermal local loading forming of TA15 alloy.

2 Experimental

TA15 titanium alloy used in this study has the following chemical compositions (mass fraction, %) of 6.06 Al, 2.08 Mo, 1.32 V, 1.86 Zr, 0.3 Fe, balance Ti. Its β-transus temperature is 1263 K. The initial microstructure is shown in Fig. 2, which consists of about 60% α_p and β_t.

An analogue experiment (Fig. 3 [10]) that can reflect the deformation characteristics of local loading forming was carried out in this work. It included two

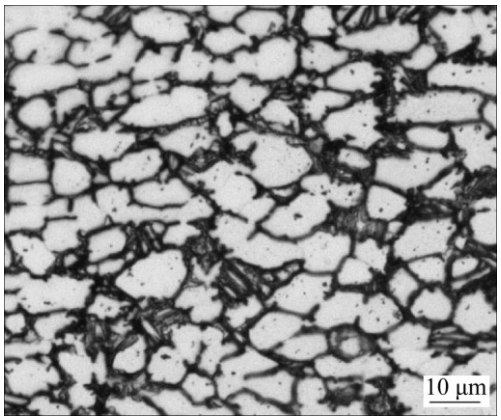

Fig. 2 Original microstructure of billet

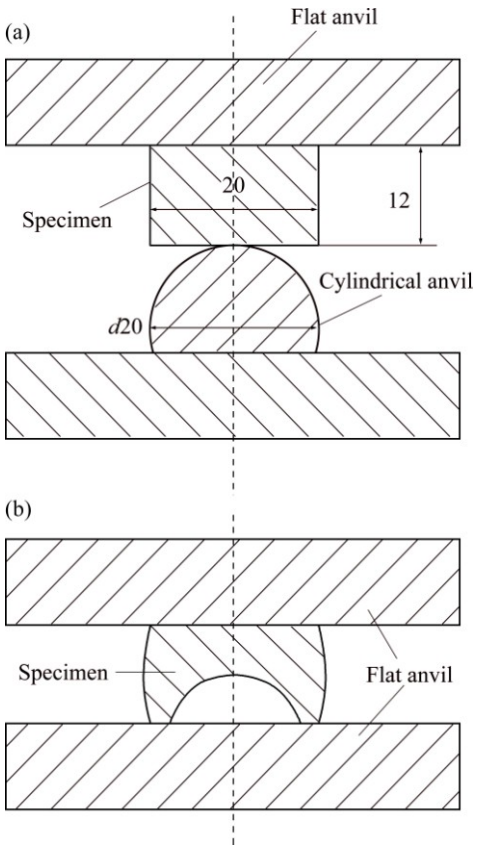

Fig. 3 Analogue experiment of local loading forming [10] (unit: mm): (a) First loading step; (b) Second loading step

loading steps in one loading pass. In each loading step, the specimen and anvils were heated to the deformation temperature at 12 K/min, held for 15 min, compressed isothermally at a nominal strain rate of 0.01 s^{-1} and then air cooled. The middle of the specimen was deformed in the first loading step, while the two sides of the specimen were highly deformed in the second loading step. The deformation temperatures in the first (T_1) and second (T_2) loading steps ranged in 1183−1253 K and 1203−1223 K, respectively. The reduction rates were 30%, 50% and 70%, which indicates the height reduction rate of final formed sample. Figure 4 shows the specimen deformed to 50% reduction after the local loading experiment. The heat treatment route after isothermal local loading was 1083 K, 1 h, AC. At last, the specimen was quartered along the two symmetric planes and prepared for metallographic observation.

In the authors' previous work [11], FE simulation was applied to calculating the local strains for microstructure analysis. Figure 4(b) shows the simulated sample, which closely matches the experimental result. The simulated strain histories (Table 1 [3]) of Regions A−C (marked in Fig. 5 [3]) suggest that they could

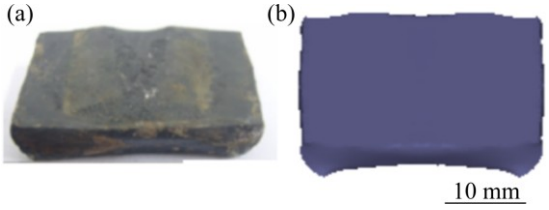

Fig. 4 Samples formed by local loading [11]: (a) Experimental result; (b) Simulated result

Table 1 Strain at microstructure observation locations (Fig. 5) of local loading formed samples [3]

Reduction rate/%	Strain in first loading step			Strain in second loading step		
	A	*B*	*C*	*A*	*B*	*C*
30	0.52	0.26	0.10	0.10	0.26	0.44
50	0.98	0.56	0.26	0.26	0.49	0.86
70	1.53	0.66	0.22	0.40	0.84	1.29

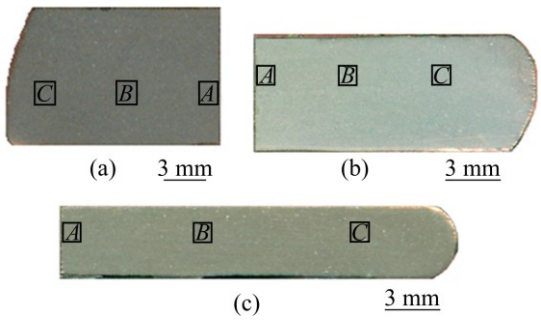

Fig. 5 Microstructure observation locations for samples deformed to different reductions [3]: (a) 30%; (b) 50%; (c) 70%

reflect the deformation characteristics of the first-loading region, transitional region and second-loading region, respectively. Thus, Regions A−C in Fig. 5 are taken as microstructure observation locations. Their effective strains in the second loading step will be used in the microstructure modelling in Section 4.

3 Development mechanisms and rules of tri-modal microstructure

To reveal the development process and rules of tri-modal microstructure, staged local loading experiments were conducted. The microstructure change in transitional region under condition of T_1=1243 K, T_2=1203 K and reduction rate of 70% is taken as an example to illustrate the development process of tri-modal microstructure, as shown in Fig. 6. In the heating of the first loading step, the allotropic transformation of $\alpha \rightarrow \beta$ proceeds, leading to obvious decrease of the α_p content. As a result, the microstructure before deformation is composed of a certain content of α_p and β phases (Fig. 6(b)). During the deformation and cooling process, the content and morphology of α_p change little, while fine secondary α produces in β phase. So, the bi-modal microstructure was generated after the first loading step, as shown in Fig. 6(c). In the heating of the second loading step, some secondary α in β_t is not transformed to β phase but becomes α_l (Fig. 6(d)), because the temperature of the second loading step is lower than that of the first loading step. During the subsequent deformation, α_l phases would gradually rotate themselves perpendicular to the compression direction, thus changing the spatial orientation disorder of α_l (Fig. 6(e)). Besides, some α_l would get globularization, i.e., dynamic globularization. During cooling, β_t would produce, obtaining the tri-modal microstructure after the second loading step (Fig. 6(e)). In the annealing, α_p and α_l would get coarsening slightly due to the precipitation and mergence of α phase, which makes the contents of α_p and α_l both increase a little. In addition, the static globularization of α_l would occur in the annealing, as shown in Fig. 6(f).

It can be found that the content variation of α_p, generation of α_l, spatial orientation change of α_l and globularization of α_l are four important microstructure phenomena in the development of tri-modal microstructure, which greatly influence the final microstructure parameters. Therefore, their dependences on the processing conditions should be revealed and caught in the microstructure modelling. According to the results of staged experiment, the influencing laws of processing on the parameters of tri-modal microstructure, including the volume fraction of α_p (f_{α_p}), volume fraction of α_l (f_{α_l}), spatial orientation disorder index of α_l (D_{α_l}) and

globularization fraction of α_l (f_g), are summarized in Table 2. The quantitative experiment results and influence laws will be described in detail in the microstructure modelling (Section 4).

4 Model of tri-modal microstructure

The common approaches for microstructure prediction of metals include the empirical methods, advanced statistical methods (such as the ANN [12]), physically based ISV methods [13] and direct simulation approaches (such as cellular automaton model [14,15]). As mentioned above, the development process of tri-modal microstructure is very complex. Moreover, some underlying microstructure evolution mechanisms, such as the change of spatial orientation of α_l, are still not fully understood. Thus, it is extremely difficult to model the tri-modal microstructure using the physically based ISV methods or direct simulation approaches. The empirical method links the microstructure parameters and processing parameters explicitly with empirical equations, in which the underlying mechanisms are not required. Thus, the empirical method was applied to modelling the tri-modal microstructure in this work.

4.1 Model of volume fraction of equiaxed α

As presented in Table 2, the content change of α_p can be divided into two stages. In Stage 1, i.e., the first loading step, the f_{α_p} significantly decreases with the increase of temperature. Moreover, the contents of α_p in various loading regions with different strains are very close. This means that temperature is the only key

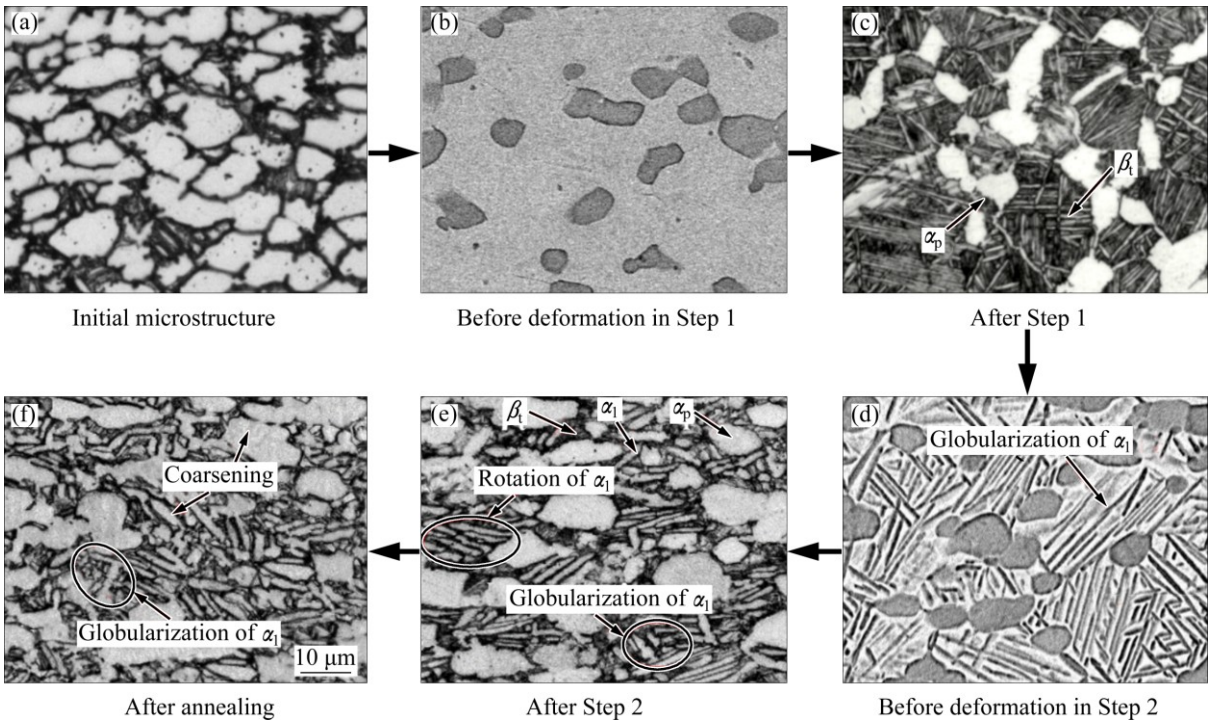

Fig. 6 Development process of tri-modal microstructure in isothermal local loading forming (Step 1 and Step 2 represent first and second loading steps, respectively)

Table 2 Key influence factors and laws for parameters of tri-modal microstructure

Parameter	Key evolution process	Key factor	Influencing law
f_{α_p}	Stage 1: f_{α_p} significantly changes in LS_1	T_1	f_{α_p} decreases with increase of T_1
	Stage 2: f_{α_p} increases by (4.98±1.25)% in LS_2 and AP	–	–
f_{α_l}	Stage 1: α_l produces in heating and holding of LS_2	T_1, T_2	f_{α_l} increases with (T_1−T_2) and T_1
	Stage 2: f_{α_l} increases by (8.31±2.60)% in AP	–	–
D_{α_l}	D_{α_l} changes in deformation of LS_2	S_2	D_{α_l} increases with S_2
f_g	Stage 1: Dynamic globularization of α_l occurs in LS_2	S_2, T_2	f_{dg} increases with S_2 and T_2
	Stage 2: Static globularization of α_l occurs in AP	S_2	f_{sg} increases with S_2

LS_1, LS_2 and AP represent the first loading step, the second loading step and the annealing process, respectively. S_2 represents the strain in the second loading step. f_{dg} and f_{sg} denote the dynamic and static globularization fractions of α_l, respectively

influencing factor for the f_{α_p}. Figure 7 shows the f_{α_p} at different temperatures after the first loading step. In Stage 2, i.e., the second loading step and annealing, the f_{α_p} slightly increases because of the precipitation and mergence of α phase. It should be noted that the increments of α_p content locate in the range of (4.98±1.25)%, which vary little with the processing conditions in this work.

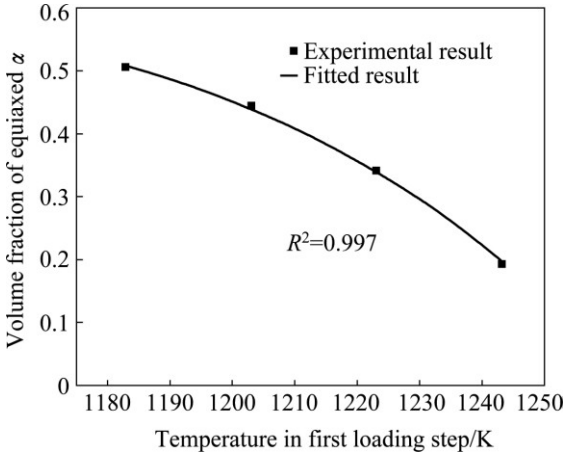

Fig. 7 Variation of volume fraction of α_p (f_{α_p}) with temperature in first loading step

According to the above evolution rules, an empirical equation (Eq. (1)) was applied to fitting the volume fraction of α_p after the first loading step. In Eq.(1), $f^1_{\alpha_p}$ represents the volume fraction of α_p after Stage 1, f_0 and f_1 are fitted material constants, T_β is the β-transus temperature. This equation has been widely used to correlate the deformation temperature and volume fraction of α_p in the hot working of titanium alloy, as reported in Ref. [16]. Figure 7 shows the fitted result. It can be seen that the experimental dada were well fitted by Eq. (1) with Adj. R^2 of 0.997 and the average error of 1.51%. The fitted f_0 and f_1 are 0.68 and 0.0174, respectively.

$$f^1_{\alpha_p} = f_0\left\{1-\exp[-f_1(T_\beta - T_1)]\right\} \quad (1)$$

The final f_{α_p} can be obtained by adding the value after Stage 1 ($f^1_{\alpha_p}$) and the increment in Stage 2. The average increment value (4.98%) was used in this work. Then, the final f_{α_p} can be calculated as follows:

$$f_{\alpha_p} = 0.68\left\{1-\exp[-0.0174(1263 - T_1)]\right\} + 0.0498 \quad (2)$$

GAO et al [3] pointed out that the temperature of the first loading step (T_1) is required to locate in the near-β region to obtain tri-modal microstructure. Thus, the range of T_1 in Eq. (1) is set as 1228−1258 K.

4.2 Model of volume fraction of lamellar α

Similar to α_p, the evolution of α_l content can also be divided into two stages, as listed in Table 2. The α_l is generated in the heating of the second loading step (Stage 1). In this stage, the volume fraction of α_l is determined by the coupling effects of temperatures in two loading steps. In the annealing (Stage 2), the volume fraction of α_l also slightly increases due to the precipitation and mergence of α phase. Similarly, the increment of α_l content is also little influenced by the processing conditions, locating in the range of (8.31±2.60)%.

Considering the coupling effects of T_1 and T_2, the volume fractions of α_l after Stage 1 are fitted by the following equation:

$$f^1_{\alpha_l} = a_0(T_1/T_\beta)^{a_1}\left\{1-\exp[-a_2(T_1 - T_2)]\right\} \quad (3)$$

where a_0, a_1 and a_2 are fitted material constants. Table 3 gives the comparison of experimental and fitted results. The average error is 1.96%. The fitted a_0, a_1 and a_2 are 3.248, 8.869 and 0.0027, respectively.

Taking the average value (8.31%) as the increment in Stage 2, the final f_{α_l} is expressed as

$$f_{\alpha_l} = 3.248(T_1/T_\beta)^{8.869}\left\{1-\exp[-0.0027(T_1 - T_2)]\right\} + 0.0831 \quad (4)$$

The conventional forging from (T_β−60) to (T_β−40) K is needed in the second loading step to get tri-modal microstructure [4]. Thus, the range of T_2 in Eq. (4) was set as 1203−1223 K.

Table 3 Comparison of experimental and fitted volume fraction of α_l (f_{α_l}) after Stage 1

T_1/K	T_2/K	Experimental f_{α_l}/%	Fitted f_{α_l}/%	Error/%
1243	1223	14.06	14.82	5.44
1243	1213	22.02	21.94	0.40
1243	1203	28.85	28.86	0.04
1253	1223	23.94	23.55	1.96
1253	1203	37.54	38.22	1.96

4.3 Model of spatial orientation disorder index of lamellar α

As described in Section 3, during the deformation of the second loading step, the α_l phases would gradually rotate themselves towards the orientation perpendicular to compression direction [17], thus changing the spatial orientation disorder of α_l. For example, Fig. 8 shows the spatial orientation distribution of α_l under conditions of T_1=1243 K, T_2=1203 K and reduction rate of 50%. Here, x-axis represents the title angle between the α_l trace and compression axis, and y-axis denotes the volume fraction of α_l. The distribution of ε=0 corresponds to the microstructure prior to deformation. It can be seen from Fig. 8 that the spatial orientation distribution of α_l gradually changes from homogeneous to concentrated,

i.e., the spatial orientation disorder of α_l decreases, with the increase of strain. Moreover, the experimental results suggest that the spatial orientation disorder of α_l is mainly determined by the strain in the second loading step.

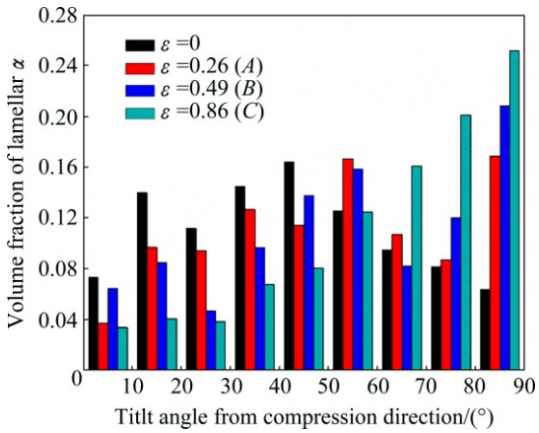

Fig. 8 Spatial orientation distribution of α_l traces relative to compression axis for sample under processing conditions of T_1=1243 K, T_2=1203 K and reduction rate of 50%

To develop the quantitative relationship between the spatial orientation disorder of α_l and deformation conditions, a spatial orientation disorder index (D_{α_l}) was proposed to measure the degree of orientation disorder:

$$D_{\alpha_l}=\sqrt{\sum_{i=1}^{9}(f_i-\overline{f})^2/9} \tag{5}$$

where f_i is the volume fraction of α_l in every 10° interval in the range of 0°−90°, and $\overline{f}=\sum_{i=1}^{9}f_i/9$. It should be kept in mind that higher D_{α_l} represents worse orientation disorder.

Based on the above analysis, only the effect of strain is considered when modelling the D_{α_l}. Figure 9 shows the variation of D_{α_l} with strain in the second loading step. According to the variation law of D_{α_l} with strain, the following equation was adopted to fit the experimental results:

$$D_{\alpha_l}=A_2+(A_1-A_2)/[1+(\varepsilon/x_0)^p] \tag{6}$$

where ε is the strain, A_1, A_2, x_0 and p are fitted material constants. From Fig. 9, It can be found that the experimental dada are well fitted by Eq. (6) with Adj. R^2 of 0.922. The fitted A_1, A_2, x_0 and p are 0.029, 0.108, 0.740 and 2.956, respectively.

4.4 Model of globularization fraction of lamellar α

As mentioned in Section 3, the globularization of α_l consists of dynamic globularization in the second loading step and static globularization in the annealing. It is suggested from Refs. [18−20] that the dynamic globularization fraction of α_l during the hot working mainly depends on the deformation temperature, strain rate, strain and thickness of α_l. In this work, the strain rate is fixed as 0.01 s^{-1}, and the thicknesses of α_l are very close under various conditions ((1.03±0.04) μm). So, it can be speculated that the deformation temperature and strain should be the key influencing factors for the dynamic globularization of α_l, which agrees with the laws concluded from experimental results (Table 2). In addition, it is found that the dynamic globularization occurs when the strain is greater than the critical strain, and its fraction approximately increases with the increase of the strain in a sigmoid way at a certain temperature. This rule has also been found in the dynamic globularization of TC11 and BT25 alloys by SONG et al [21] and MA et al [22]. They suggested that this change law can be well fitted by the Avrami type equation:

$$f_{dg}=1-\exp[-k(\varepsilon-\varepsilon_c)^n] \tag{7}$$

where f_{dg} is the dynamic globularization fraction, ε is the strain, k is the temperature-dependent kinetic constant, ε_c is the critical strain for the initiation of dynamic globularization, and n is the Avrami exponent. Thus, the Avrami type equation was also applied to fitting the variation of dynamic globularization fraction of α_l with strain, as shown in Fig. 10. In this work, the globularization was taken to be an α-phase morphology with aspect ratio less than 2.5. It can be seen that the fitting results agree well with the experimental results at various temperatures. Table 4 [3] lists the fitted material constants at different temperatures.

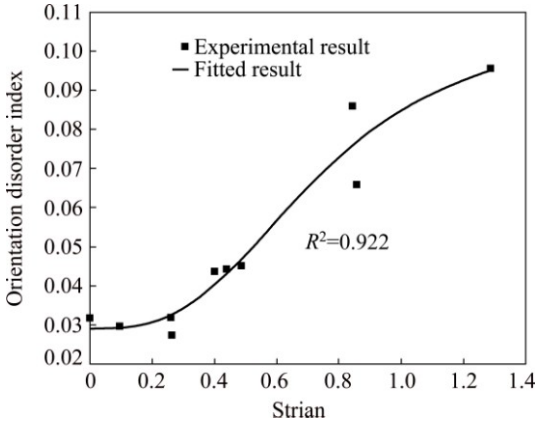

Fig. 9 Spatial orientation disorder index of α_l vs strain in second loading step

From Table 4, it can be found that the fitted parameters change with temperature. To predict the dynamic globularization, it is necessary to build the relationship between the fitted parameters and temperature. Based on the variation rules of fitted parameters with temperature, the following three

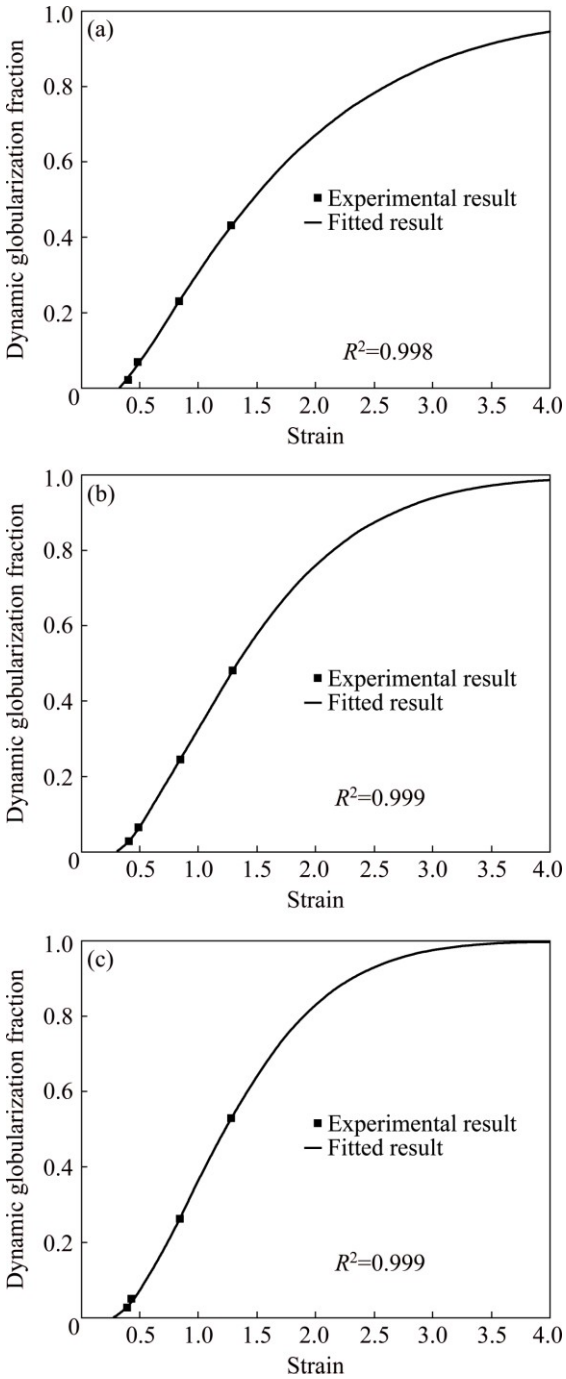

Fig. 10 Dynamic globularization fraction of α_l vs strain in second loading step at different temperatures: (a) 1203 K; (b) 1213 K; (c) 1223 K

equations were proposed to fit their relationships:

$$\ln \varepsilon_c = b_1(1/T_2) + b_0 \tag{8}$$

$$k = c_1(T_2/T_\beta) + c_0 \tag{9}$$

$$n = d_0 + d_1(T_2/T_\beta) + d_2(T_2/T_\beta)^2 \tag{10}$$

where b_0, b_1, c_0, c_1, d_0, d_1 and d_2 are fitted parameters. Table 5 shows the fitted parameters for Eqs. (8)−(10). The calculated results by Eqs. (8)−(10) are very close to the original data, as shown in Table 4. By the combination of Eqs. (7)−(10), the dynamic globularization fractions of α_l under different temperatures and strains can be predicted.

As for the static globularization of α_l in the annealing, it is revealed that if the strain in the second loading step exceeds the critical strain for dynamic globularization, the static globularization will produce. Moreover, the static globularization fraction increases with the increase of the strain but changes little with temperature. Figure 11 shows the static globularization fractions at various $\varepsilon-\varepsilon_c$ values in the second loading step. It can be seen that the static globularization fraction is approximately linearly related to $\varepsilon-\varepsilon_c$, thus, Eq. (11) is applied to fitting their relationship. It can be seen from Fig. 11 that the experimental dada are well fitted by Eq. (11) with Adj. R^2 of 0.934. The fitted k_1 and b are 0.082 and 0.006, respectively.

$$f_{sg} = k_1(\varepsilon - \varepsilon_c) + b \tag{11}$$

where f_{sg} is the static globularization fraction, k_1 and b are fitted material constants.

Based on the above analysis, the total globularization fraction of α_l can be expressed as

$$f_g = f_{dg} + f_{sg} = \begin{cases} 1-\exp[-k(\varepsilon-\varepsilon_c)^n] + k_1(\varepsilon-\varepsilon_c) + b, & \varepsilon \geq \varepsilon_c \\ 0, & \varepsilon < \varepsilon_c \end{cases} \tag{12}$$

where ε_c, k and n can be calculated by Eqs. (8)−(10), respectively. It should be noted that when the strain in the second loading step is smaller than the critical strain, neither the dynamic globularization nor the static globularization occurs.

Table 4 Fitted parameters in Avrami type equation at various temperatures [3]

Temperature/K	Fitted ε_c	Fitted k	Fitted n	Calculated ε_c by Eq. (8)	Calculated k by Eq. (9)	Calculated n by Eq.(10)
1203	0.320	0.590	1.230	0.320	0.589	1.230
1213	0.280	0.650	1.452	0.282	0.650	1.452
1223	0.249	0.712	1.624	0.249	0.712	1.625

Table 5 Fitted parameters for Eqs. (8)−(10)

b_0	b_1	c_0	c_1	d_0	d_1	d_2
−16.465	18434.964	−6.763	7.719	−383.985	777.742	−391.933

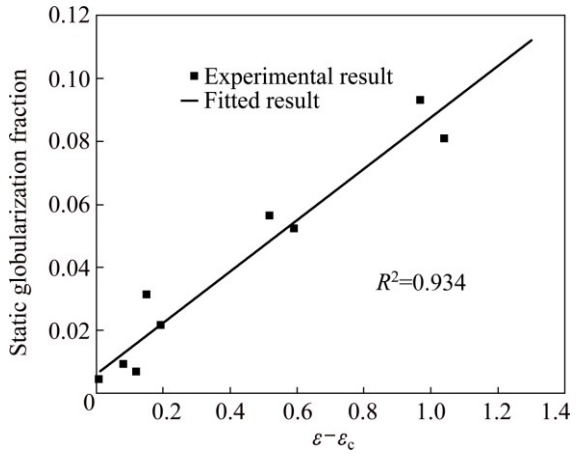

Fig. 11 Static globularization fraction of α_l vs $\varepsilon-\varepsilon_c$ of second loading step

5 Application of tri-modal microstructure model

In the isothermal forming, the temperature of workpiece almost keeps uniform and unchanged in each loading step. So, the f_{α_p} and f_{α_l} in the final tri-modal microstructure are also uniform in the whole workpiece, which can be directly predicted by Eqs. (2) and (4), respectively. Figure 12 shows the variations of f_{α_p} and f_{α_l} with the temperatures of two loading steps within 1228 K≤T_1≤1258 K, 1203 K≤T_2≤1223 K.

However, the predictions of D_{α_l} and f_g are more difficult compared with the f_{α_p} and f_{α_l} owing to the severe unequal deformation during local loading forming. To predict the distributions of D_{α_l} and f_g on the workpiece, it is required to obtain the strain distribution first. Incorporating the microstructure model and FE model is a feasible way to solve this problem. Thus, the models for D_{α_l} and f_g (Eqs. (6) and (12), respectively) were combined with FE model by user subroutine of DEFORM-3D.

To verify its accuracy, the integrated model was used to simulate the isothermal local loading experiment of TA15 alloy (Section 2). The prediction of macroscopic deformation has been validated by the sample shape in Ref. [11]. In this work, the microstructure observations were carried out in different regions to verify the integrated microstructure prediction model. The verification experiment was conducted under the condition of T_1=1253 K, T_2=1213 K and reduction rate of 50%, which was not applied in the microstructure modelling in Section 4. Figure 13 shows the distribution of strain in the second loading step. Figures 14(a) and (b) show the FE-based prediction results of D_{α_l} and f_g of the final tri-modal microstructure, respectively.

The microstructures at four points (P_1−P_4 in Fig. 13) with different strains were characterized to validate the

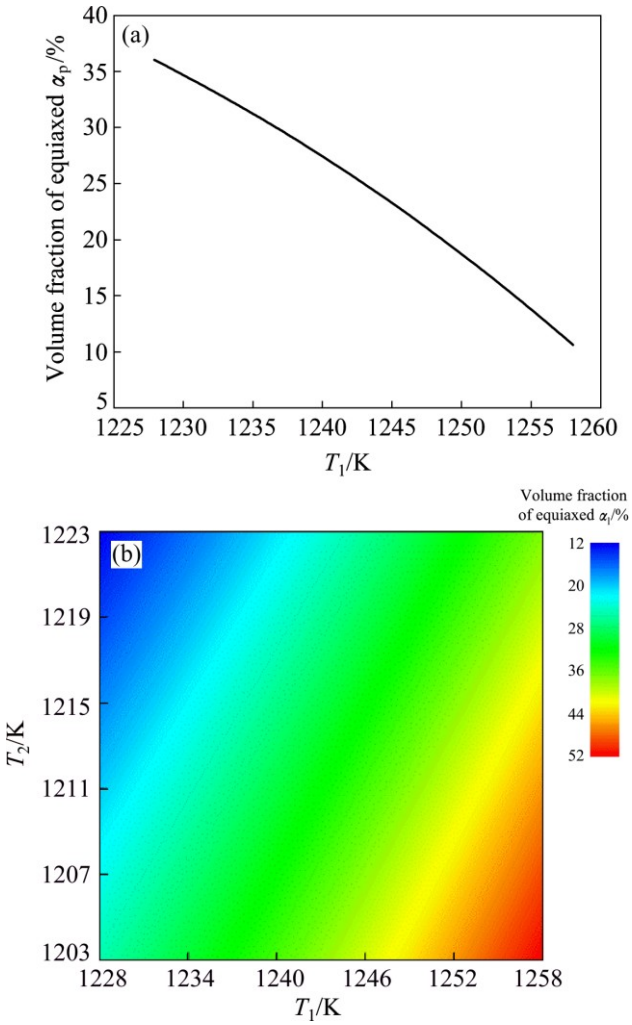

Fig. 12 Variations of volume fractions of α_p (a) and α_l (b) with temperatures of two loading steps

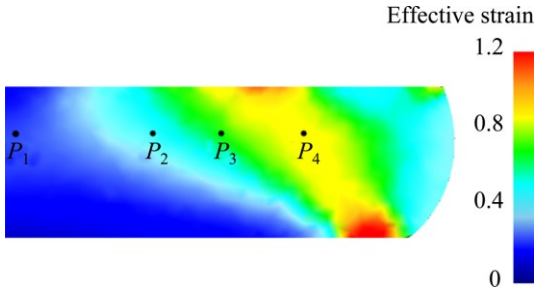

Fig. 13 Distribution of strain in second loading step

simulation results, as shown in Fig. 15. It can be seen that the f_{α_p} and f_{α_l} of the four points are very close. Quantitative analyses indicate that the average measured f_{α_p} and f_{α_l} of the four points are 17.32% and 37.15%, respectively. By Eqs. (2) and (4), the f_{α_p} and f_{α_l} are predicted as 15.84% and 39.29% with the errors of 8.5% and 5.8%, respectively. Meanwhile, the predicted D_{α_l} and f_g are also compared to the experimental results, as given in Table 6. It can be found that the simulated results all agree well with the experimental results. The average

prediction errors for D_{α_1} and f_g are 8.4% and 7.6%, respectively. The above comparisons indicate that the developed microstructure model and its combination with FE model are effective in the prediction of tri-modal microstructure during the isothermal local loading forming of TA15 alloy.

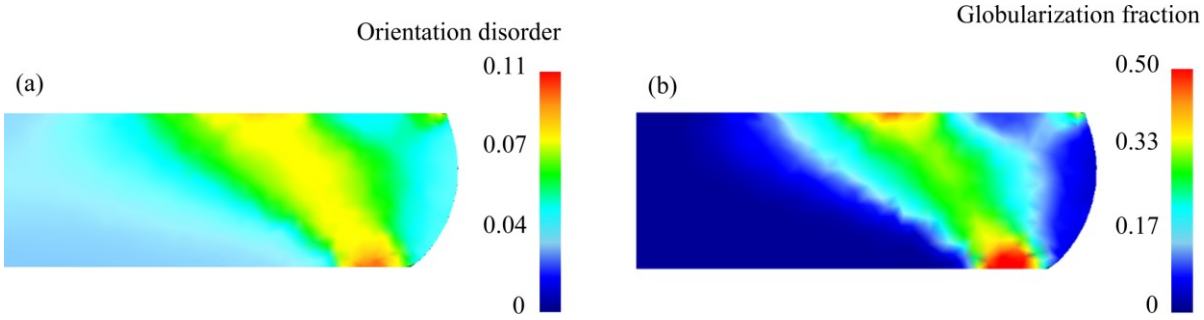

Fig. 14 FE-based prediction results of orientation disorder index (a) and globularization fraction (b) of α_1 of final tri-modal microstructure

Fig. 15 Microstructures in verification experiment under conditions of T_1=1253 K, T_2=1213 K and reduction rate of 50% at different locations: (a) P_1; (b) P_2; (c) P_3; (d) P_4

Table 6 Comparison of microstructure parameters between experimental and predicted results

Point in Fig. 13	Strain	Orientation disorder index of α_1			Globularization fraction of α_1		
		Experimental	Predicted	Error/%	Experimental	Predicted	Error/%
P_1	0.26	0.033	0.032	3.0	0	0	–
P_2	0.49	0.041	0.047	14.6	0.096	0.088	8.3
P_3	0.69	0.068	0.064	5.9	0.214	0.202	5.7
P_4	0.86	0.070	0.077	10.0	0.283	0.308	8.8

6 Conclusions

1) The content variation of equiaxed α, generation of lamellar α, spatial orientation change of lamellar α and globularization of lamellar α are four important microstructure evolution phenomena in the development of tri-modal microstructure during isothermal local loading forming of titanium alloy. The dependences of these microstructure phenomena on processing conditions are quantitatively summarized.

2) The microstructure model including the volume fractions of equiaxed α and lamellar α, spatial orientation disorder of lamellar α and globularization fraction of lamellar α, was established to correlate the parameters of tri-modal microstructure under the local loading processing conditions.

3) The developed microstructure model was incorporated with FE model to predict the tri-modal microstructure in the isothermal local loading forming of TA15 alloy. The prediction results were validated by experimental microstructure observations. The prediction model would provide basis for the quantitative control of tri-modal microstructure and performance in the isothermal local loading forming of titanium alloy.

References

[1] ZHANG D W, YANG H. Development of transition condition for region with variable-thickness in isothermal local loading process [J]. Transactions of Nonferrous Metals Society of China, 2014, 24: 101−108.

[2] YANG H, FAN X G, SUN Z C, GUO L G, ZHAN M. Recent developments in plastic forming technology of titanium alloys [J]. Science China: Technological Sciences, 2011, 54: 490−501.

[3] GAO P F, FAN X G, YANG H. Role of processing parameters in the development of tri-modal microstructure during isothermal local loading forming of TA15 titanium alloy [J]. Journal of Materials Processing Technology, 2017, 239: 160−171.

[4] ZHOU Y G, ZENG W D, YU H Q. An investigation of a new near-beta forging process for titanium alloys and its application in aviation components [J]. Materials Science and Engineering A, 2005, 393: 204−212.

[5] ZHANG D W, YANG H, SUN Z C, FAN X G. Influences of fillet radius and draft angle on local loading process of titanium alloy T-shaped components [J]. Transactions of Nonferrous Metals Society of China, 2011, 21: 2693−2704.

[6] LI Z Y, YANG H, SUN Z C, TANG Z. Research on marco-microcosmic deforming in isothermal local loading transition region for large-scale complex integral components of TA15 titanium alloy [J]. Rare Metal Materials and Engineering, 2008, 37: 1516−1521. (in Chinese)

[7] FAN X G, YANG H, GAO P F. Through-process macro-micro finite element modeling of local loading forming of large-scale complex titanium alloy component for microstructure prediction [J]. Journal of Materials Processing Technology, 2014, 214: 253−266.

[8] GAO Y, SUN Z C, YANG H. Model for predicting microstructure of TA15 titanium alloy in near β forging based on improved BP neural network [J]. Journal of Plasticity Engineering, 2012, 19: 49−55. (in Chinese)

[9] SUN Z C, WANG X Q, ZHANG J, YANG H. Prediction and control of equiaxed α in near-β forging of TA15 Ti-alloy based on BP neural network: For purpose of tri-modal microstructure [J]. Materials Science and Engineering A, 2014, 591: 18−25.

[10] FAN X G, GAO P F, YANG H. Microstructure evolution of the transitional region in isothermal local loading of TA15 titanium alloy [J]. Materials Science and Engineering A, 2011, 528: 2694−2703.

[11] GAO P F, YANG H, FAN X G. Quantitative analysis of the microstructure of transitional region under multi-heat isothermal local loading forming of TA15 titanium alloy [J]. Materials & Design, 2011, 32: 2012−2020.

[12] XU J W, ZENG W D, JIA Z Q, SUN X, ZHOU J H. Prediction of static globularization of Ti-17 alloy with starting lamellar microstructure during heat treatment [J]. Computational Materials Science, 2014, 92: 224−230.

[13] ZHU S, YANG H, GUO L G, GU R J. Investigation of deformation degree and initial forming temperature dependences of microstructure in hot ring rolling of TA15 titanium alloy by multi-scale simulations [J]. Computational Materials Science, 2012, 65: 221−229.

[14] JIN Z, CUI Z S. Modelling the effect of initial grain size on dynamic recrystallization using a modified cellular automata and a adaptive response surface method [J]. Journal of Materials Science and Technology, 2010, 26: 1063−1070.

[15] GRONG Ø, SHERCLIFF H R. Microstructural modelling in metals processing [J]. Progress in Materials Science, 2002, 47: 163−282.

[16] FAN X G, YANG H, GAO P F. Prediction of constitutive behavior and microstructure evolution in hot deformation of TA15 titanium alloy [J]. Materials & Design, 2013, 51: 34−42.

[17] MA F, LU W, QIN J, ZHANG D. Microstructure evolution of near-α titanium alloys during thermomechanical processing [J]. Materials Science and Engineering A, 2006, 416: 59−65.

[18] SEMIATIN S L, SEETHARAMAN V, WEISS I. Flow behavior and globularization kinetics during hot working of Ti−6Al−4V with a colony alpha microstructure [J]. Materials Science and Engineering A, 1999, 263: 257−271.

[19] SEMIATIN S L, BIELER T R. The effect of alpha platelet thickness on plastic flow during hot working of Ti−6Al−4V with a transformed microstructure [J]. Acta Materialia, 2011, 49: 3565−3573.

[20] MIRONOV S, MURZINOVA M, ZHEREBTSOV S, SALISHCHEV G A, SEMIATIN S L. Microstructure evolution during warm working of Ti−6Al−4V with a colony-α microstructure [J]. Acta Materialia, 2009, 57: 2470−2481.

[21] SONG H W, ZHANG S H, CHENG M. Dynamic globularization kinetics during hot working of a two-phase titanium alloy with a colony alpha microstructure [J]. Journal of Alloys and Compounds, 2009, 480: 922−927.

[22] MA X, ZENG W, TIAN F, ZHOU Y G. The kinetics of dynamic globularization during hot working of a two phase titanium alloy with starting lamellar microstructure [J]. Materials Science and Engineering A, 2012, 548: 6−11.

钛合金等温局部加载复杂热变形历史下的三态组织预测

高鹏飞，杨 合，樊晓光，雷珍妮，蔡 杨

西北工业大学 材料学院 凝固技术国家重点实验室，西安 710072

摘 要：建立钛合金等温局部加载三态组织预测模型，以实现三态组织参数与性能的定量调控。逐工步的 TA15 钛合金等温局部加载实验表明，三态组织形成中存在 4 个重要组织演化现象：条状 α 相的生成、各组成相含量变化、条状 α 相取向变化及条状 α 相的球化。基于实验结果，总结了工艺条件对上述 4 种组织演化现象的定量影响规律，在此基础上建立了联系三态组织参数(等轴 α 相含量、条状 α 相含量、条状 α 相取向分布混乱度指数、条状 α 相的球化分数)与成形条件的三态组织预测模型。然后，将组织模型嵌入有限元模拟软件，建立了基于有限元的等温局部加载三态组织预测模型。通过实验组织观测验证了模型的可靠性与准确性，说明本文作者建立的三态组织模型及其与有限元模型的集成可以有效地预测 TA15 钛合金等温局部加载三态组织参数。

关键词：钛合金；等温局部加载成形；复杂热变形历史；三态组织建模

(Edited by Wei-ping CHEN)